PAPER

NJC
www.rsc.org/njc

Heterocyclic quinol-type fluorophores.† Dramatic solid-state fluorescence enhancement behaviour of imidazoanthraquinol-type clathrate hosts upon inclusion of various kinds of organic solvent molecules‡

Yousuke Ooyama and Katsuhira Yoshida*

Department of Material Science, Faculty of Science, Kochi University, Akebono-cho, Kochi, 780-8520, Japan. E-mail: kyoshida@cc.kochi-u.ac.jp; Fax: (+81) 88-844-8359

Received (in St. Louis, MO, USA) 28th July 2004, Accepted 12th July 2005
First published as an Advance Article on the web 2nd August 2005

The crystals of novel imidazoanthraquinol-type clathrate hosts exhibit sensitive colour change and fluorescence enhancement behaviour upon enclathration of various kinds of organic solvent molecules. The optical changes are greatly dependent on the identity of the enclathrated guest molecules. To elucidate the enclathrated guest effects on the fluorescence properties of the crystals, the X-ray crystal structures of the guest-free and guest-inclusion compounds have been determined. On the basis of the spectral data and the crystal structures, the effects of the enclathrated guest on the solid-state photophysical properties of the clathrate compounds are discussed.

Introduction

Chromogenic receptors that exhibit sensitive changes in colour and fluorescence intensity upon formation of host–guest complexes have received considerable attention owing to their fundamental photophysical properties and their potential applications in analytical and material sciences.[1] Some trials that intended to apply clathrate formation to a sensing system for detection of organic solvent molecules have been made.[2–4] A few clathrate hosts that can exhibit sensitive colour changes upon enclathration of guest molecules are known.[5] However, very little is known about fluorescent clathrate hosts.[6]

Recently, we have developed several novel fluorophores that have guest-inclusion ability in the crystalline state.[7–9] The solid-state fluorescence intensity of the clathrate hosts was enhanced to various degrees depending on the enclathrated guest molecules. Such phenomena are of great interest for the development of new chemosensors and solid-state emissive materials. In connection with this research, we have further developed novel isomeric pairs of imidazoanthraquinol-type fluorophores (**2** and **3**) exhibiting tautomerism (**A** and **B**) on the imidazole ring in solution and in the crystalline state.

In this paper, we report the guest inclusion ability of **2a** for various kinds of organic solvent molecules and its concomitant fluorescence enhancement behaviour in the crystalline state. The changes in the solid-state fluorescence excitation and emission spectra and in the X-ray crystal structure upon formation of the clathrate compounds have been elucidated. The relationship between the observed solid-state photophysical properties and the X-ray crystal structures is discussed.

Results and discussion

Inclusion ability in the crystalline state

In designing clathrate hosts, it is required that specific structural units such as a rigid backbone, bulky substituents, and anchor groups are combined.[10–12] In order to create new clathrate hosts having fluorescence emissive ability, we employed our original heterocyclic quinol-type fluorophore as a rigid backbone with anchor groups such as a hydroxyl group, a carbonyl group, and an imidazole ring. Thus, we have designed and synthesized 2-[(4-diethylamino)phenyl]imidazo[5,4-*a*]anthraquinol derivatives (**2a–2b** and **3a–3c**) from compound **1** (Scheme 1). The details for the synthesis of these compounds were reported in our previous paper.[7a] We have found that the quinol **2a** yields various host–guest inclusion compounds in stoichiometric ratios with various organic solvent molecules. Although the quinol **2b** also gave a host–guest inclusion compound with ethanol, it did not form inclusion compounds with other organic solvents such as 1-butanol, 1,4-dioxane, acetonitrile, benzene, acetone. It is considered that the larger substituent (R) adjacent to the anchor groups in **2** is unfavourable towards fixing guest molecules. On the other hand, the quinols **3a–3c** did not exhibit any inclusion ability. These results suggest that the hydroxyl group adjacent to the imidazole ring is effective in fixing guest molecules in the crystalline state. The characteristics of the guest free and various inclusion crystals obtained by recrystallization of the quinols are summarized in Table 1. Compared to the guest-free crystals, the colour of the guest-inclusion crystals varied from orange to light yellow and a dramatic fluorescence enhancement was observed.

The thermal analyses (TG and DTA) were performed to investigate the thermal stability of the clathrate crystals and the resulting thermograms are shown in Fig. 1. The guest release patterns were considerably different depending on the identity of enclathrated solvent molecules. After releasing solvent molecules, the host **2a** began to decompose at around 180 °C without melting. The guest release temperatures for 1,4-dioxane and alcohols were higher than their original boiling points. In contrast, the acetone and acetonitrile inclusion crystals did not show a sharp weight loss process; these crystals showed a

† Part 4. For Part 3, see: ref. 17.
‡ Electronic supplementary information (ESI) available: Table S1 Crystal data and structure refinement parameters for the guest-free and the guest inclusion compounds of **2a**. See http://dx.doi.org/10.1039/b411591k

DOI: 10.1039/b411591k

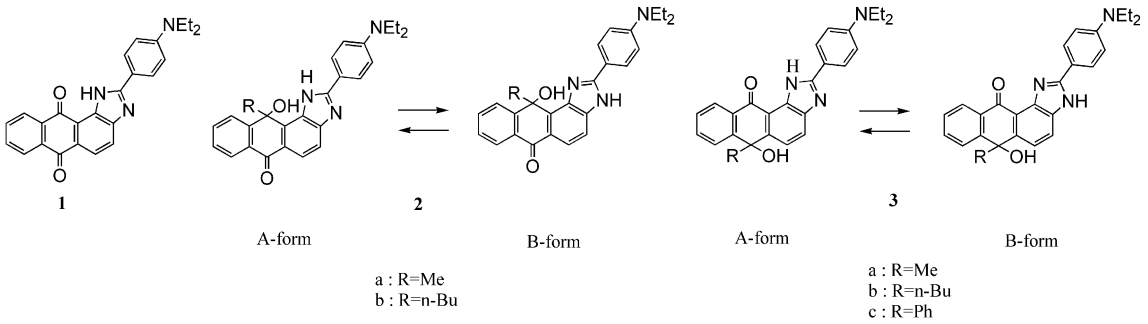

Scheme 1

Table 1 Host–guest molar ratios, crystal form, and colour of the guest-free and guest-inclusion crystals of the quinols

Host	Guest	Host : Guest (mole ratio)	Crystal form	Crystal colour	Recrystallization solvent
	None	1 : 0	Prism	Orange	Chloroform–*n*-hexane
	Ethanol	1 : 1	Needle	Yellow	99% Ethanol
	1-Butanol	1 : 1	Needle	Yellowish orange	1-Butanol
	1-Popanol	1 : 1	Needle	Yellowish orange	1-Propanol
2a	*t*-Butyl alcohol	1 : 2	Prism	Yellow	*t*-Butyl alcohol
	1,4-Dioxane	2 : 1	Needle	Yellow	1,4-Dioxane
	Diethyl ether	2 : 1	Prism	Yellow	Diethyl ether
	Acetonitrile	1 : 1	Prism	Light yellow	Acetonitrile
	Benzene	2 : 1	Needle	Yellow	Benzene
	Acetone	2 : 1	Needle	Yellow	Acetone
	Propionic acid	1 : 1	Leaflet	Yellow	Propionic acid
2b	None	1 : 0	Prism	Orange	Chloroform–*n*-hexane
	Ethanol	2 : 1	Needle	Yellow	99% ethanol
3a	None	1 : 0	Prism	Orangish brown	Chloroform–*n*-hexane
3b	None	1 : 0	Prism	Orange	Chloroform–*n*-hexane
3c	None	1 : 0	Prism	Orange	Chloroform–*n*-hexane

gradual release of the guest molecules in room temperature and concomitantly the colour changes from light yellow to an initial orange of the guest-free crystals. However, the 1,4-dioxane and alcohols inclusion crystals were very stable and did not release the guest molecules during several months at room temperature.

Solid-state fluorescence enhancement behaviour upon formation of guest-inclusion crystals

In order to investigate the effect of clathrate formation on the solid-state photophysical properties, the fluorescence excitation and emission spectra of the guest-free and the guest-inclusion crystals were measured. A typical example of the spectra recorded at the corresponding excitation and emission maxima is shown in Fig. 2. Compared to the guest-free crystal, the excitation and emission maxima of the guest-inclusion crystals exhibit a blue shift and the fluorescence intensity is enhanced to various degrees depending on the identity of the enclathrated guest molecules. The guest-free host crystal exhibits relatively weak fluorescence with emission maximum at 567 nm, while the guest-inclusion crystals exhibit much stronger fluorescence intensity with the emission maximum blue shifted to around 532–505 nm. In comparison with the guest-free crystal, the fluorescence intensities of the guest-inclusion crystals were *ca.* 8-fold in diethyl ether-, *ca.* 11-fold in 1-butanol-, *ca.* 23-fold in 1,4-dioxane-, *ca.* 46-fold in ethanol-, and *ca.* 68-fold in *t*-butanol-inclusion crystals, respectively.

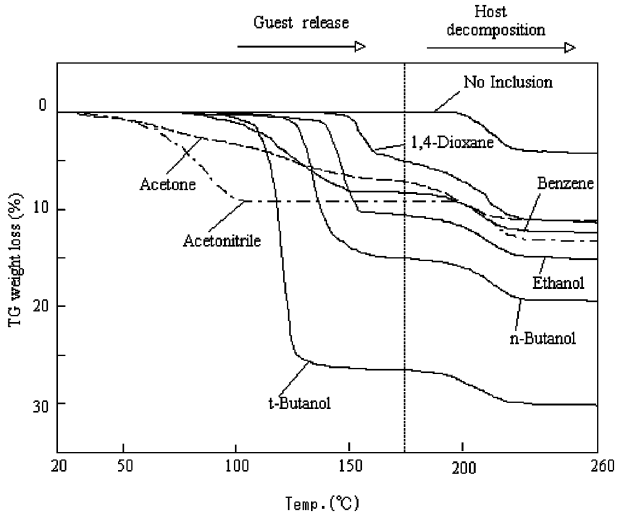

Fig. 1 TG curves for the host–guest inclusion crystals of **2a** at a heating rate 5 °C min^{-1}. Host (**2a**) : guest; 2 : 1 (acetone), 1 : 1 (acetonitrile), 2 : 1 (benzene), 2 : 1 (1,4-dioxane), 1 : 1 (ethanol), 1 : 1 (1-butanol), 1 : 2 (*t*-butanol).

It was also found that the final spectra were obtained *via* a solid-gas contact. For example, the time-dependent changes in the excitation and fluorescence spectra of the guest-free crystals upon exposure to ethanol or 1-butanol vapour at 30 °C are shown in Fig. 3 and 4. In the case of ethanol, the initial excitation band at 520 nm shifted to 512 nm and the fluorescence band at 567 nm shifted to shorter wavelength with an increase in fluorescence intensity until 1.5 h (H : G = 1 : 0.5), and then the excitation band at 512 nm gradually disappears and the fluorescence maximum continually shifted to shorter wavelength with an increase in fluorescence intensity. It took about 4–5 h to reach the final saturated excitation and emission spectra which were in good agreement with the spectra of the clathrate compound (**2a** · ethanol = 1 : 1). In contrast, when 1-butanol was used instead of ethanol, the time-dependent changes in the excitation and fluorescence spectra were quite different. The initial excitation band at 520 nm shifted to 509 nm and the fluorescence band at 567 nm decreased in fluorescence intensity without change of the wavelength until 2.5 h (H : G = 1 : 0.5), and then the excitation band at 509 nm shifted to 480 nm and the fluorescence maxima at 567 nm shifted to around

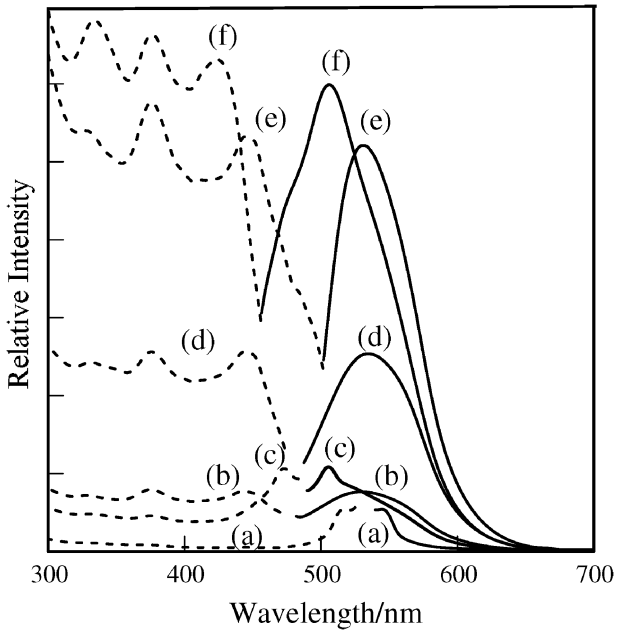

Fig. 2 Excitation (···) and emission (—) spectra of the guest-free and guest-inclusion crystals of **2a**: (a) **2a** (guest-free), $\lambda_{ex} = 520$, $\lambda_{em} = 567$ nm, (b) **2a** · diethyl ether (2 : 1), $\lambda_{ex} = 444$, $\lambda_{em} = 532$ nm, (c) **2a** · 1-butanol (1 : 1), $\lambda_{ex} = 473$, $\lambda_{em} = 505$ nm, (d) **2a** · 1,4-dioxane (2 : 1), $\lambda_{ex} = 445$, $\lambda_{em} = 526$ nm, (e) **2a** · ethanol (1 : 1), $\lambda_{ex} = 451$, $\lambda_{em} = 528$ nm, (f) **2a** · *t*-butanol (1 : 2), $\lambda_{ex} = 424$, $\lambda_{em} = 505$ nm.

band at 510 nm. The final spectra were in good agreement with the spectra of crystals of the corresponding clathrate compound (**2a** · 1-butanol = 1 : 1). These results indicate that the photophysical spectral changes upon the solid-gas contact reflect strictly the changes in molecular packing induced by the enclathrated guest molecules in the crystals.

Relation between the solid-state fluorescence properties and X-ray crystal structures of various clathrate compounds of 2a

In order to make clear the big differences in the solid-state fluorescence enhancement upon enclathration of organic solvent molecules, we have determined the X-ray crystal structures of the guest-free and the guest-inclusion compounds obtained by recrystallization. The experimental details and crystal data are listed in Table S1‡. The crystal systems were a monoclinic space group $P2_1/c$ with $Z = 4$ for guest-free **2a** and **2a** · 1-butanol, a monoclinic space group $P2_1/n$ with $Z = 4$ for **2a** · ethanol and **2a** · *t*-butanol, a triclinic space group $P\bar{1}$ with $Z = 2$ for **2a** · 1,4-dioxane, and an orthorhombic space group $Pna2_1$ with $Z = 8$ for **2a** · diethyl ether.

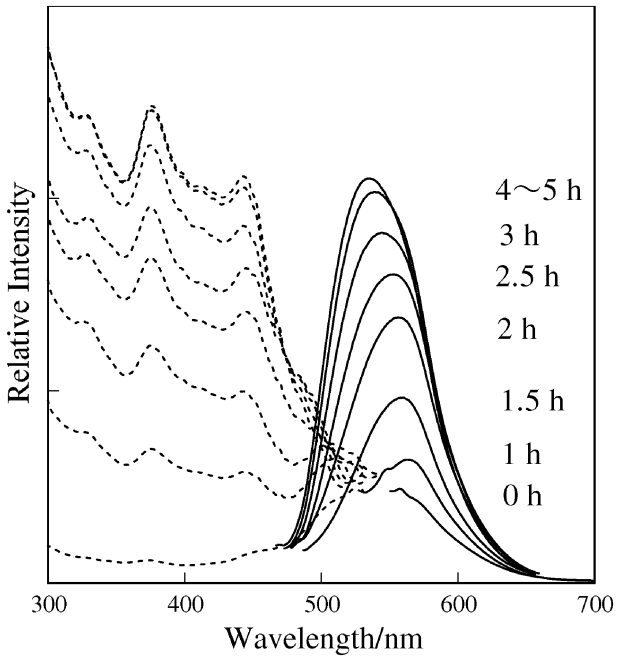

Fig. 3 Time-dependent spectral changes of the guest-free crystal of **2a** upon exposure to ethanol vapour at 30 °C; the excitation (···) and emission (—) spectra were recorded at their corresponding emission and excitation maxima.

Fig. 5–10 show the X-ray crystal structures of the guest-free and the guest-inclusion compounds. The tautomeric forms (A and B) of imidazole ring of **2a** in the crystalline state were changed depending on the enclathrated guest molecules. The tautomeric form of **2a** is A-form in the crystals of the guest-free, **2a** · 1-butanol, **2a** · *t*-butanol, and **2a** · 1,4-dioxane and B-form in the crystals of **2a** · ethanol and **2a** · diethyl ether. These results indicate that the host **2a** can include various guest molecules by changing the toutomeric form on the imidazole ring.

The phenyl group of **2a** is twisted out of the plane of the heterocyclic quinol skeleton by 2–17° except for **2a** · *t*-butanol (31.2°). The packing structures demonstrate that the all guest-inclusion compounds except for **2a** · diethyl ether are built up from a centrosymmetric cluster unit, and that the molecules are arranged in a "herringbone" fashion in the crystals of the guest-free compound, **2a** · ethanol, **2a** · 1-butanol, **2a** · *t*-butanol, and **2a** · diethyl ether and in "bricks in a wall" fashion in the crystal of **2a** · 1,4-dioxane.

Fig. 5(a) shows the molecular packing structure for the crystal of **2a**.[17] The crystal of **2a** is built up by a centrosymmetric dimer unit which is composed of a pair of enantiomers bound cofacially by two intermolecular hydrogen bonds between the hydroxyl oxygen and imidazole nitrogen through the hydroxyl proton, which is realized on both sides of the molecules (O(1)H(1)···N(2)* angle = 159(6)°, O(1)···N(2)* distance = 2.991(5) Å) as shown in Fig. 5(b). The intramolecular hydrogen bond formation is also observed between the imidazole amino proton and the hydroxyl oxygen in each quinol molecule (N(1)H(2)···O(1) angle = 117(2)°, N(1)···O(1) distance = 2.887(3) Å). A side view of the dimer unit and its upside view together with the non-bonded interatomic distances of less than 3.60 Å are shown in Fig. 5(c) and (d), respectively. The π-stacking between a pair of quinol enantiomers is covering through the whole molecule from the donor unit of *p*-diethylaminophenyl moiety to the acceptor unit of imidazoanthraquinol moiety, there are 18 (= 9 × 2) short interatomic π–π contacts in the pair of enantiomers. The interplanar distance between the imidazole plates is *ca.* 3.39 Å, which suggests strong π–π interactions. Such strong intermolecular interactions between the fluorophores have been considered to induce the large red-shift of the absorption[13–15] and fluorescence maxima and an intense fluorescence quenching[8,16] in the solid state.

The crystal of **2a** · 1-butanol (H : G = 1 : 1) is built up by the hydrogen bonded cluster unit composed of a pair of enantiomers of the host **2a** and two 1-butanol guest molecules (Fig. 6(a)). As shown in Fig. 6(b), the hydroxyl proton of **2a** is directing toward the oxygen of the guest (O(1)H(1)···O(3) angle = 170(1)°, O(1)···O(3) distance = 2.758(3) Å), and the hydroxyl proton of the guest is directing toward the iminonitrogen of another host molecule (O(3)H(26)···N(2)* angle = 175(1)°, O(3)···N(2)* distance = 2.776(3) Å). The intermolecular hydrogen bonds are realized on both sides of the cluster unit. The intramolecular hydrogen bonds are also observed between the hydroxyl oxygen and the amino proton of imidazole ring in each host molecule (N(1)H(8)···O(1) angle = 118(9)°, N(1)···O(1) distance = 2.861(3) Å). The close π–π contacts between a pair of the quinol enantiomers are covering the whole molecular skeleton, there are 14 (= 7 × 2) short interatomic π–π contacts of less than 3.6 Å. The interplanar

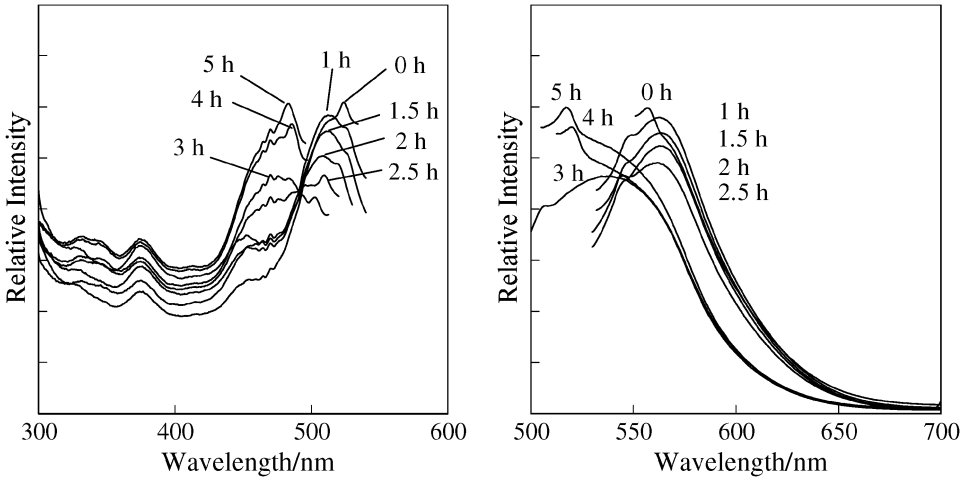

Fig. 4 Time-dependent excitation and emission spectral changes of the guest-free crystal of **2a** upon exposure to 1-butanol vapour at 30 °C; (a) excitation spectra and (b) emission spectra were recorded at their corresponding emission and excitation maxima.

distance between the two quinol plates is *ca.* 3.46 Å, which suggests strong π–π interactions (Fig. 6(c) and 6(d)).

On the other hand, the crystal of **2a** · 1,4-dioxane[7b] (H : G = 2 : 1) is built up by the hydrogen bonded unit of a pair of enantiomers of the host and 1,4-dioxane molecules are included into the cavities formed among the units (Fig. 7(a)). As shown in Fig. 7(b), the intermolecular hydrogen bond between the hydroxyl oxygen and imino nitrogen of imidazole ring through the hydroxyl proton is realized on both sides of the host molecules (O(1)H(1)···N(2)* angle = 155(3)°, O(1)···N(2)* distance = 3.012(3) Å). The amino proton of the imidazole ring have two proton acceptors and become bifurcated-donor hydrogen to form the three-centred hydrogen bonding arrangements with the intramolecular hydroxyl oxygen (N(1)H(2)···O(1) angle = 107(2)°, N(1)···O(1) distance = 2.914(2) Å) and with the oxygen atom of 1,4-dioxane guest (N(1)H(1)···O(3) angle = 169(2)°, N(1)···O(3) distance = 3.109(2) Å). The side and top views of the cluster unit is drawn in Fig. 7(c) and 7(d). There are 16 (= 8 × 2) short interatomic π–π contacts of less than 3.6 Å, which also suggest π–π interactions. The interplanar distance between the two host plates is *ca.* 3.50 Å, which is enlarged in comparison with the case of **2a** · 1-butanol.

The crystal of **2a** · ethanol[7b] (H : G = 1 : 1) is built up by a cluster unit composed of a pair of the host enantiomers and

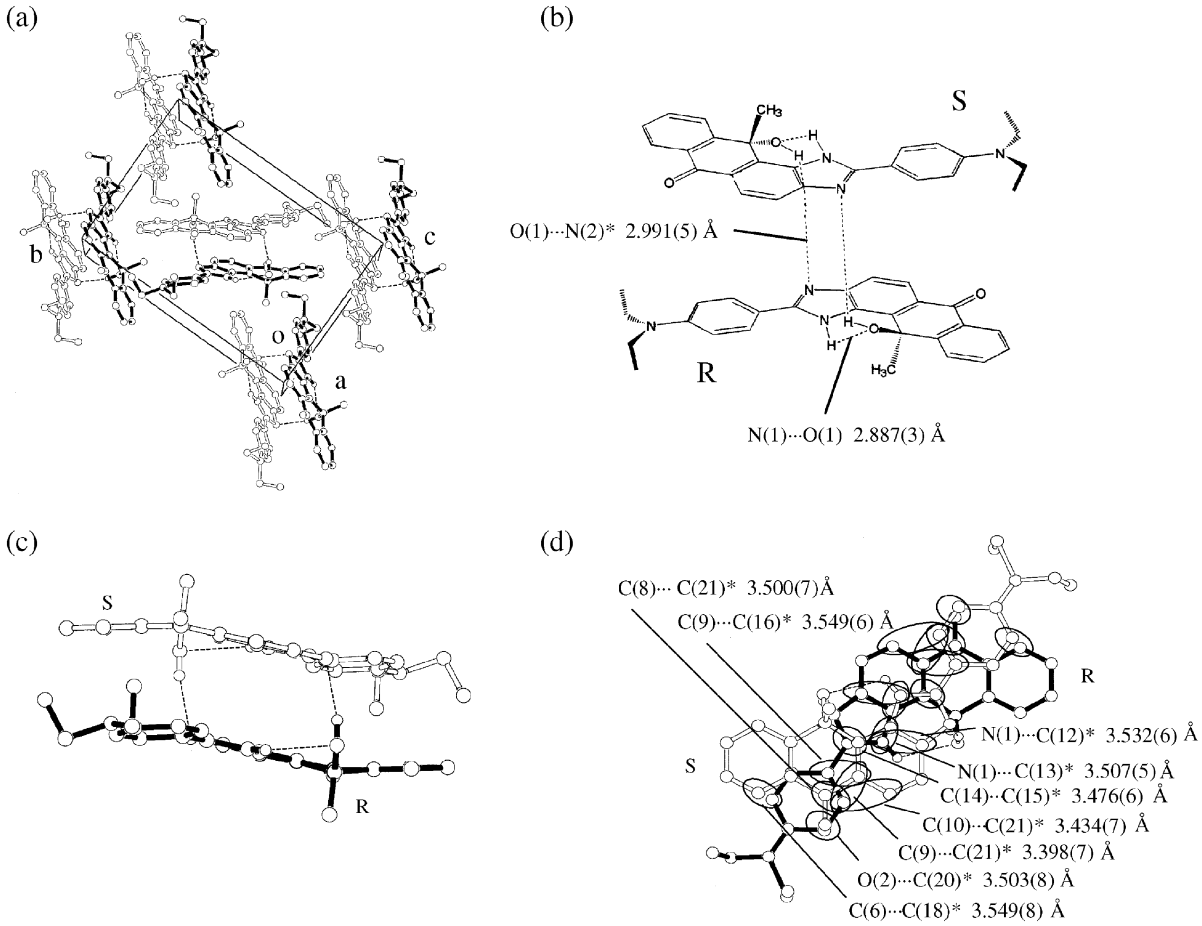

Fig. 5 Crystal packing and hydrogen bonding pattern of **2a**: (a) a stereoview of the molecular packing structure, and (b) a schematic structure, (c) a side view, and (d) a top view of the pairs of enantiomers.

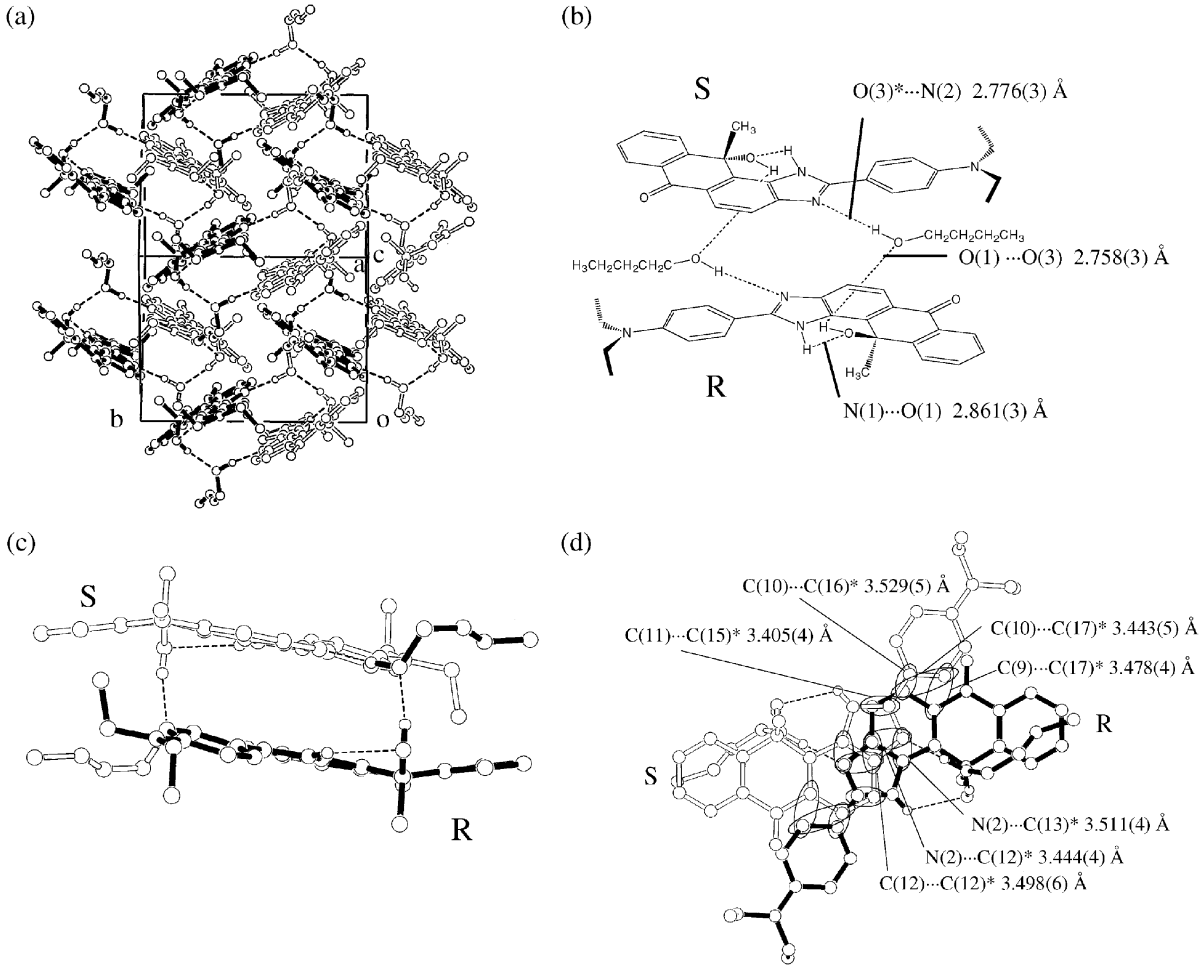

Fig. 6 Crystal packing and hydrogen bonding pattern of **2a** · 1-butanol (1 : 1): (a) a stereoview of the molecular packing structure, and (b) a schematic structure, (c) a side view, and (d) a top view of a cluster unit.

two ethanol molecules (Fig. 8(a)). An amino proton of an imidazole ring is directing toward the oxygen of the guest (N(2)*H(2)*···O(3) angle = 164(2)°, N(2)*···O(3) distance = 2.780(2) Å) and the hydroxyl proton of the guest is directing toward a hydroxyl oxygen of another host molecules (O(3)H(26)···O(1) angle = 162(7)°, O(3)···O(1) distance = 2.757(1) Å) as shown in the Fig. 8(b) and (c). The intermolecular hydrogen bonds are realized on both sides of the host molecules to form a four-member cluster unit. Intramolecular hydrogen bonding is also observed between the hydroxyl proton and the imino nitrogen in each host molecule (O(1)H(1)···N(1) angle = 143(2)°, O···O distance = 2.777(2) Å). The number of short interatomic contacts of less than 3.6 Å in the cluster unit and between the clusters is 16 (= 8 × 2) and 6 (= 3 × 2), respectively (Figs. 8(d) and (e)). The interplanar distance between the two host plates is *ca.* 3.61 in the cluster unit and 3.63 Å between the clusters. It is considered from these data that the crystal of **2a** · ethanol exhibits comparatively strong fluorescent intensity because of the enlarged interplanar distance in comparison with the case of **2a** · 1-butanol and **2a** · 1,4-dioxane.

Fig. 9(a) shows the crystal of **2a** · *t*-butanol (H : G = 1 : 2) which is built up by a six-membered cluster unit composed of a pair of the host enantiomers and four *tert*-butyl alcohol molecules. As shown in Fig. 9(b), a pair of enantiomers and two *tert*-butyl alcohol molecules are bound by four hydrogen bonds, where the hydroxyl proton of the host is directing toward the oxygen of the guest (O(1)H(1)···O(3) angle=177(3)°, O(1)···O(3) distance = 2.660(3) Å) and the hydroxyl proton of the guest is directing toward imino nitrogen of another host molecule (O(3)H(26)···N(2)* angle = 158(5)°, O(3)···N(2)* distance = 2.801(3) Å). In addition, the rest two *tert*-butyl alcohol molecules are bound to each of the enantiomers by two intermolecular hydrogen bonds in which the amino proton of the imidazole ring is directing toward the oxygen of the guest (N(1)H(2)···O(4) angle = 169(3)°, N(1)···O(4) distance = 3.051(3) Å), and the hydroxyl proton of the guest is directing toward the hydroxyl oxygen of the same host molecules (O(4)H(36)···O(1) angle = 169(4)°, O(4)···O(1) distance = 2.729(3) Å). There are 6 (= 3 × 2) short interatomic contacts of less than 3.6 Å between the host molecules (Fig. 9(c) and (d)). The interplanar distance between the two plates is *ca.* 3.73 Å, which indicates a considerable destruction of the π–π interactions.

A comparison of the above five crystal structures confirms that the strength of the π–π interactions decrease in the following order: **2a**(guest-free) > **2a** · 1-butanol > **2a** · 1,4-dioxane > **2a** · ethanol > **2a** · *t*-butanol. As seen Fig. 2, the solid-state fluorescence intensity is the reverse order. These results confirm that the differences in the destruction of the host–host π–π interactions by enclathration of the guest molecules are reflected on the solid-state fluorescence intensity of the crystals.

Interestingly, in the case of **2a** · diethyl ether (H : G = 2 : 1), there are two crystallographically independent molecules in the crystal (Fig. 10(a)). Intramolecular hydrogen bonding is also observed between the hydroxyl proton and imino nitrogen of each crystallographically independent molecule (O(1)H(1)···N(1) and O(3)H(26)···N(4) angle = 143(5) and 126(5)°, O(1)···N(1) and O(3)···N(4) distance = 2.861(1) and 2.822(7) Å, respectively). Moreover, it is interestingly to see that the crystal is built up with one-dimensional chains con-

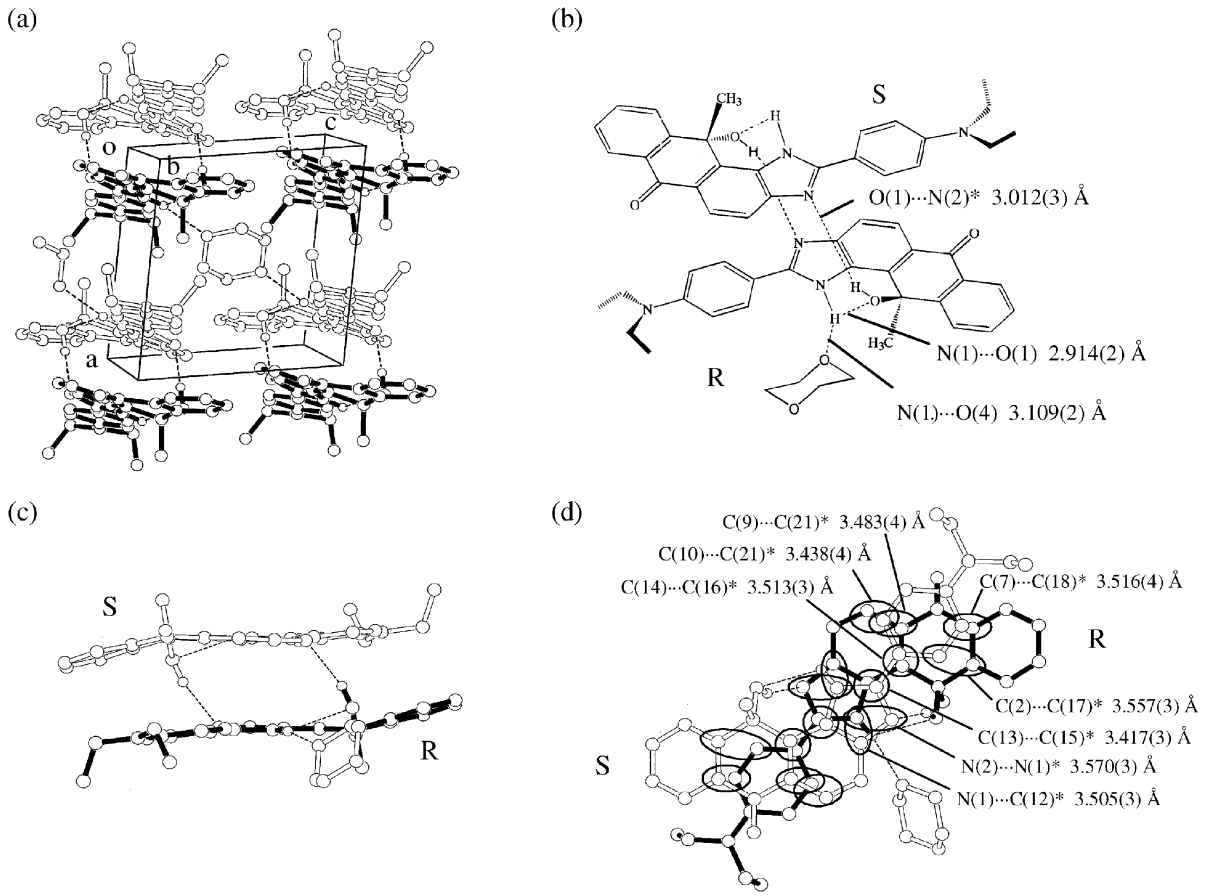

Fig. 7 Crystal packing and hydrogen bonding pattern of **2a** · 1,4-dioxane (2 : 1): (a) a stereoview of the molecular packing structure, and (b) a schematic structure, (c) a side view, and (d) a top view of a cluster unit.

sisting of *R*- or *S*-enantiomers that are formed through the long-range intermolecular hydrogen bonding between the neighbouring crystallographically independent molecules (N(2)H(2)···O(3) and N(5)H(27)···O(1) angle = 153(8) and 156(9)°, N(2)···O(3) and N(5)···O(1) distance = 2.934(9) and 2.940(8) Å) as shown in Fig. 10(b) and (c). Ether molecules are included into the cavities formed between the neighbouring one-dimensional chains. The close π-overlapping is observed between the diethylaminophenyl moieties of the neighbouring *R*- and *S*-enantiomers, where there are 6 short interatomic contacts of less than 3.6 Å (Fig. 10(d)). The intermolecular distance between the two plates is *ca.* 3.55 Å, which suggests a weak π–π interaction in comparison with the cases of **2a** · 1-butanol and **2a** · 1,4-dioxane. However, the solid-state fluor-

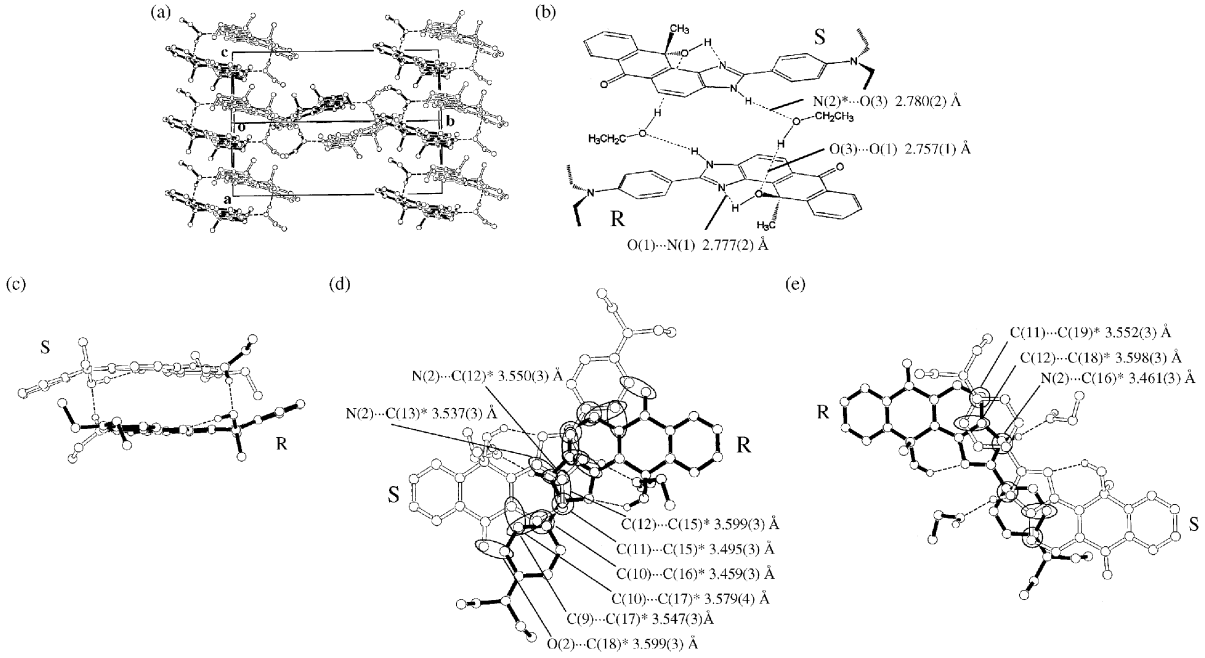

Fig. 8 Crystal packing and hydrogen bonding pattern of **2a** · ethanol: (a) a stereoview of the molecular packing structure, and (b) a schematic structure, (c) a side view, (d) a top view of a cluster unit, and (e) a top view of short interatomic contacts between a cluster.

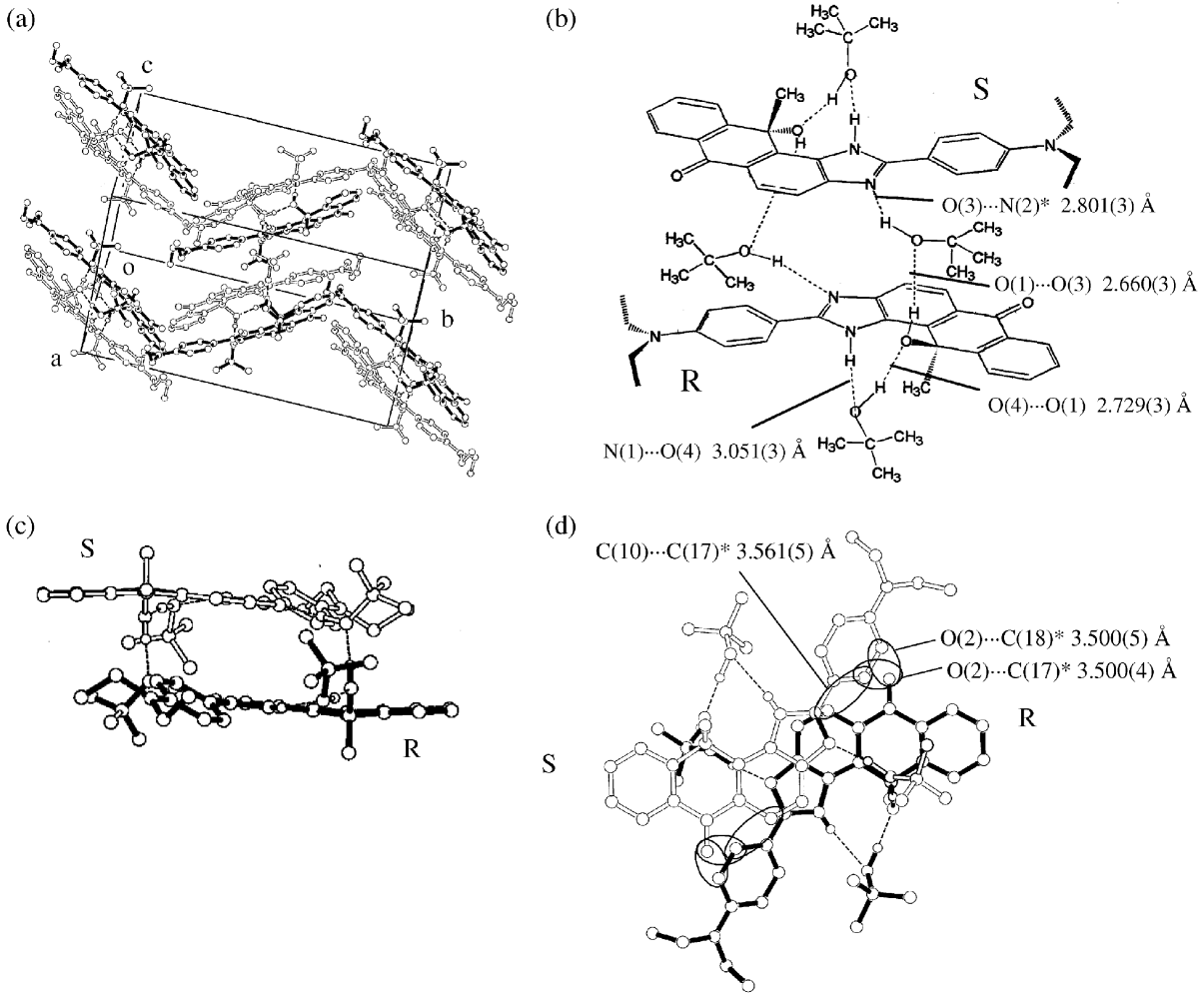

Fig. 9 Crystal packing and hydrogen bonding pattern of **2a** · *t*-butanol (1 : 2): (a) a stereoview of the molecular packing structure, and (b) a schematic structure, (c) a side view, and (d) a top view of a cluster unit.

escence intensity of **2a** · diethyl ether is weaker than that of **2a** · 1-butanol and **2a** · 1,4-dioxane as shown Fig. 2. These findings confirm that the fluorescence quenching of **2a** · diethyl ether is attributed to the long-range intermolecular hydrogen bonds connecting the fluorophores. Such findings that the existence of long-range intermolecular hydrogen bonds forming one-dimensional chains of the fluorophores results in a strong solid-state fluorescence quenching are also observed in other crystals.[9,17]

Conclusion

It was found that the fluorophore **2a** can include various guest molecules in the crystalline state by changing the tautomeric form on the imidazole ring. A dramatic fluorescence enhancement and a blue-shift of the absorption and fluorescence wavelength maxima are observed depending on the enclathrated guest molecules. From the comparison of the X-ray crystal structures of the guest-free and several clathrate compounds, we have concluded the destruction of the π–π interactions and the intermolecular hydrogen bonds binding fluorophores by the enclathrated guest molecules are the main reason for the guest-dependent fluorescence enhancement and the blue-shift of the absorption and fluorescence maxima of the crystals. Furthermore, it is confirmed that an existence of long-range intermolecular hydrogen bonds forming one-dimensional chains of fluorophores lead to a strong solid-state fluorescence quenching behaviour.

Experimental

Elemental analyses were measured with a Perkin Elmer 2400 II CHN analyzer. Thermogravimetry (TG) and differential thermal analysis (DTA) spectra were performed on a Rigaku TG 8120. Single-crystal X-ray diffraction was performed on a Rigaku AFC7S diffractometer. Fluorescence emission and excitation spectra were measured with a JASCO FP-777 spectrometer. For the measurement of the solid-state fluorescence excitation and emission spectra of the crystals, Jasco FP-1060 attachment was used. ^{1}H NMR spectra were recorded on a JNM-LA-400 (400 MHz) FT NMR spectrometer with tetramethylsilane (TMS) as an internal standard.

Preparation of guest-inclusion crystals of 2a

The host compound **2a** was dissolved with heating in the respective guest solvent. The solution was filtered and kept for a few days at room temperature. The crystals that formed were collected by filtration. The host : guest stoichiometric ratio of the inclusion compounds was determined by means of ^{1}H NMR integration and CHN analysis.

X-ray crystallographic studies

The reflection data were collected at 23 ± 1 °C on a Rigaku AFC7S four-circle diffractometer by 2θ–ω scan technique, and using graphite-monochromated Mo-Kα (λ = 0.710 69 Å) radiation at 50 kV and 30 mA. In all case, the data were corrected for Lorentz and polarization effects. A correction for

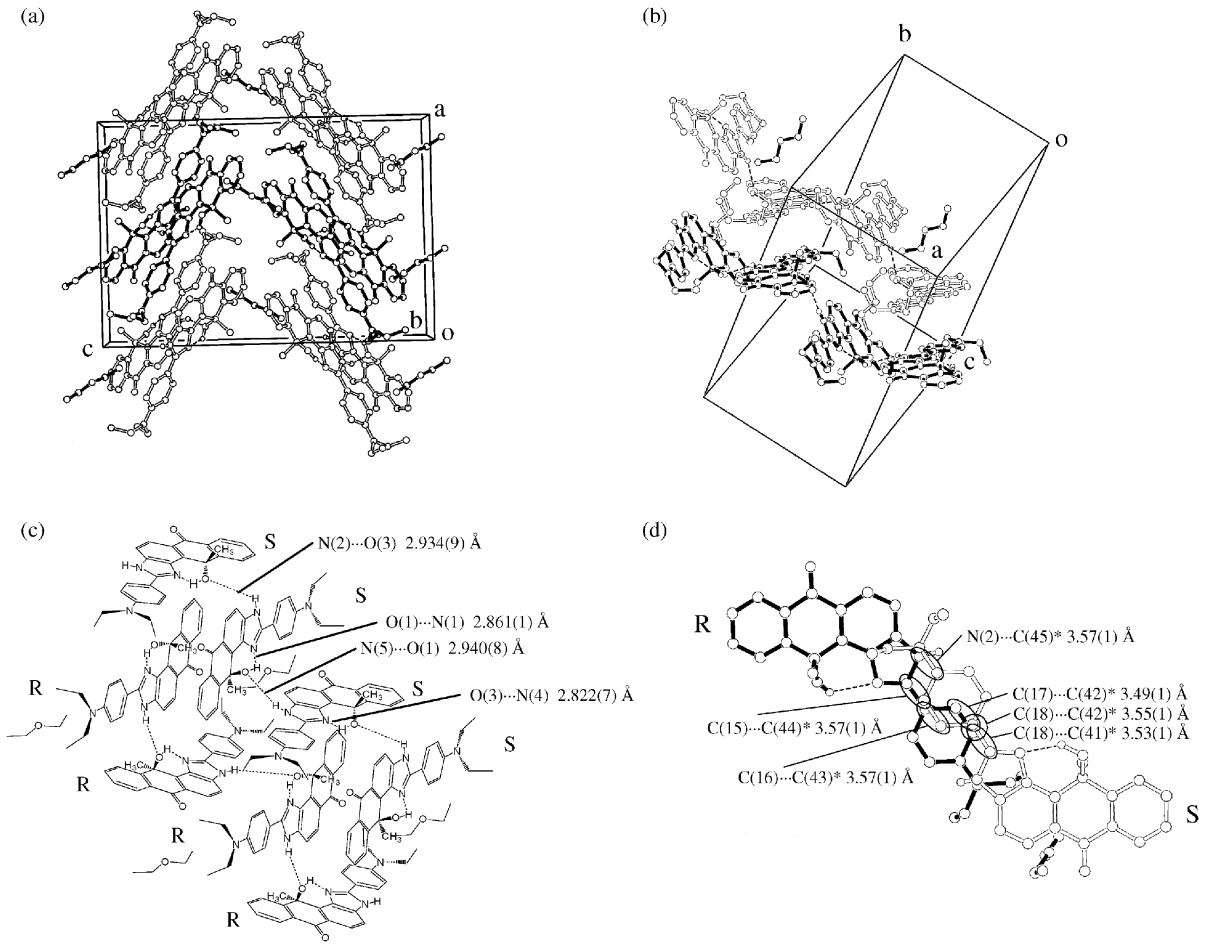

Fig. 10 Crystal packing and hydrogen bonding pattern of **2a** · diethyl ether (2 : 1): (a) a stereoview of the molecular packing structure, and (b) intra- and intermolecular hydrogen bonds between enantiomers, (c) a schematic structure, and (d) nearest contact between enantiomers.

secondary extinction was applied. Crystal data, data collection and refinement parameters are summarized in Table S1‡. The reflection intensities were monitored by three standard reflections for every 150 reflections. An empirical absorption correction based on azimuthal scans of several reflections was applied. All calculations were performed using the teXsan[18] crystallographic software package of Molecular Structure Corporation.

Crystal structure determination of 2a

Crystals of **2a** were recrystallized from dichloromethane–*n*-hexane as air-stable orange prisms. The one selected had approximate dimensions 0.45 × 0.25 × 0.45 mm. The transmission factors ranged from 0.97 to 1.00. The crystal structure was solved by direct methods using SIR 92.[19] The structures were expanded using Fourier techniques.[20] The non-hydrogen atoms were refined anisotropically. Some hydrogen atoms were refined isotropically, the rest were fixed geometrically and not refined.

Crystal data. $C_{26}H_{25}N_3O_2$, $M = 411.50$, monoclinic, $a = 11.111(2)$, $b = 16.954(2)$, $c = 12.318(2)$ Å, $\beta = 113.97(1)^\circ$, $U = 2120.3(5)$ Å^3, $T = 296.2$ K, space group $P2_1/c$ (no. 14), $Z = 4$, μ(Mo-K$_a$) = 0.8 cm^{-1}, 3936 reflections measured, 3735 unique ($R_{int} = 0.020$) which were used in all calculations. The final R indices [$I > 2\sigma(I)$], $R1 = 0.0827$, $wR(F^2) = 0.2003$.

Crystal structure determination of 2a · ethanol

Crystal of **2a** · ethanol was recrystallized from ethanol as air-stable yellow prisms. The one selected had approximate dimensions 0.60 × 0.60 × 0.60 mm. The transmission factors ranged from 0.95 to 0.95. The crystal structure was solved by direct methods using SIR 88.[21] The structures were expanded using Fourier techniques.[20] The non-hydrogen atoms were refined anisotropically. Some hydrogen atoms were refined isotropically, the rest were fixed geometrically and not refined.

Crystal data. $C_{28}H_{31}N_3O_3$, $M = 457.57$, monoclinic, $a = 7.957(3)$, $b = 20.750(2)$, $c = 14.977(2)$ Å, $\beta = 96.81(2)^\circ$, $U = 2455.2(10)$ Å^3, $T = 296.2$ K, space group $P2_1/n$ (no. 14), $Z = 4$, μ(Mo-K$_a$) = 0.8 cm^{-1}, 4809 reflections measured, 4460 unique ($R_{int} = 0.016$) which were used in all calculations. The final R indices [$I > 2\sigma(I)$], $R1 = 0.0465$, $wR(F^2) = 0.1153$.

Crystal structure determination of 2a · 1-butanol

Crystals of **2a** · 1-butanol were recrystallized from 1-butanol as air-stable yellowish orange prisms. The one selected had approximate dimensions 0.30 × 0.80 × 0.30 mm. The transmission factors ranged from 0.98 to 0.98. The crystal structure was solved by direct methods using SIR 88.[21] The structures were expanded using Fourier techniques.[20] The non-hydrogen atoms were refined anisotropically. Some hydrogen atoms were refined isotropically, the rest were fixed geometrically and not refined.

Crystal data. $C_{30}H_{35}N_3O_3$, $M = 485.62$, monoclinic, $a = 13.277(2)$, $b = 11.943(2)$, $c = 17.664(3)$ Å, $\beta = 108.36(1)^\circ$, $U = 2658.3(8)$ Å^3, $T = 296.2$ K, space group $P2_1/c$ (no. 14), $Z = 4$, μ(Mo-K$_a$) = 0.8 cm^{-1}, 3598 reflections measured, 3462 unique ($R_{int} = 0.036$) which were used in all calculations. The final R indices [$I > 2\sigma(I)$], $R1 = 0.0537$, $wR(F^2) = 0.1332$.

Crystal structure determination of 2a · *t*-butanol

Crystal of **2a** · *t*-butanol was recrystallized from *tert*-butyl alcohol as air-stable yellow prisms. The one selected had approximate dimensions 0.20 × 0.20 × 0.65 mm. The transmission factors ranged from 0.98 to 1.0. The crystal structure was solved by direct methods using SIR 92.[19] The structures were expanded using Fourier techniques.[20] The non-hydrogen atoms were refined anisotropically. Some hydrogen atoms were refined isotropically, the rest were fixed geometrically and not refined.

Crystal data. $C_{34}H_{45}N_3O_4$, $M = 559.75$, monoclinic, $a = 9.620(2)$, $b = 23.485(2)$, $c = 15.297(2)$ Å, $\beta = 107.87(1)^\circ$, $U = 3289.3(7)$ Å^3, $T = 296.2$ K, space group $P2_1/n$ (no. 14), $Z = 4$, μ(Mo-K$_a$) = 0.7 cm^{-1}, 6166 reflections measured, 5803 unique ($R_{int} = 0.026$) which were used in all calculations. The final R indices were $R1 = 0.0593$, $wR(F^2) = 0.1292$ (all data).

Crystal structure determination of 2a · 1,4-dioxane

Crystal of **2a** · 1,4-dioxane was recrystallized from 1,4-dioxane as yellow prism, air stable. The one selected had approximate dimensions 0.40 × 0.40 × 0.70 mm. The transmission factors ranged from 088 to 1.00. The crystal structure was solved by direct methods using SIR 92.[19] The structures were expanded using Fourier techniques.[20] The non-hydrogen atoms were refined anisotropically. Some hydrogen atoms were refined isotropically, the rest were fixed geometrically and not refined.

Crystal data. $C_{28}H_{29}N_3O_3$, $M = 455.56$, triclinic, $a = 9.250(3)$, $b = 16.607(8)$, $c = 8.100(2)$ Å, $\alpha = 96.08(3)^\circ$, $\beta = 97.90(2)^\circ$, $\gamma = 96.25(3)^\circ$, $U = 1215.8(8)$ Å^3, $T = 296.2$ K, space group $P1$ (no. 2), $Z = 2$, μ(Mo-K$_a$) = 0.9 cm^{-1}, 4559 reflections measured, 4270 unique ($R_{int} = 0.009$) which were used in all calculations. The final R indices [$I > 2\sigma(I)$], $R1 = 0.0601$, $wR(F^2) = 0.1568$.

Crystal structure determination of 2a · diethyl ether

Crystasl of **2a** · diethylether were recrystallized from diethyl ether as air-stable yellow prisms. The one selected had approximate dimensions 0.40 × 0.30 × 0.60 mm. The transmission factors ranged from 0.91 to 1.00. The crystal structure was solved by direct methods using SIR 92.[19] The structures were expanded using Fourier techniques.[20] The non-hydrogen atoms were refined anisotropically. Some hydrogen atoms were refined isotropically, the rest were fixed geometrically and not refined.

Crystal data. $C_{28}H_{30}N_3O_{2.5}$, $M = 448.56$, orthorhombic, $a = 16.57(1)$, $b = 12.047(8)$, $c = 24.125(8)$ Å, $U = 4816(4)$ Å^3, $T = 296.2$ K, space group $Pna2_1$ (no. 33), $Z = 8$, μ(Mo-K$_a$) = 0.8 cm^{-1}, 4857 reflections measured, 4488 unique ($R_{int} = 0.984$) which were used in all calculations. The final R indices [$I > 2\sigma(I)$], $R1 = 0.0497$, $wR(F^2) = 0.0571$.

Acknowledgements

Y.O. was supported by research fellowships from the Japan Society for the Promotion of Science (JSPS) for young scientists.

References

1 (*a*) *Advances in Fluorescence Sensing Technology V*, ed. J. R. Lakowicz and R. B. Thompson, SPIE, Rellingham, WA, USA, 2001; (*b*) *Fluorescent and Luminescent Probes for Biological Activity*, ed. W. T. Mason, Academic Press, San Diego, USA, 2nd edn., 1999; (*c*) A. P. de Silva, H. Q. N. Gunaratne, T. Gunnlaugsson, A. J. M. Huxley, C. P. McCoy, J. T. Rademacher and T. E. Rice, *Chem. Rev.*, 1997, **97**, 1515; (*d*) E. Weber, T. Hens, Q. Li and C. W. Mak, *Eur. J. Org. Chem.*, 1999, 1115; (*e*) L. M. Leung, W. Y. Lo, S. K. So, K. M. Lee and W. K. Choi, *J. Am. Chem. Soc.*, 2000, **122**, 5640; (*f*) K. Tanaka, M. Asami and J. L. Scott, *New J. Chem.*, 2002, **26**, 378.

2 E. Weber, K. Skobridis and I. Goldberg, *J. Chem. Soc., Chem. Commun.*, 1989, 1195.

3 (*a*) N. Hayashi, K. Kuruma, Y. Mazaki, T. Imakubo and K. Kobayashi, *J. Am. Chem. Soc.*, 1998, **120**, 3779; (*b*) K. Kuruma, H.-O. Nakagawa, T. Imakubo and K. Kobayashi, *Bull. Chem. Soc. Jpn.*, 1999, **72**, 1395.

4 M. Kaftory, H. Taycher and M. Botoshansky, *J. Chem. Soc., Perkin Trans. 2*, 1998, 407.

5 (*a*) Y. Inouye and Y. Sakaino, *Bull. Chem. Soc. Jpn.*, 1986, **59**, 3295; (*b*) Y. Sakaino, T. Takizawa, Y. Inouye and H. Kakisawa, *J. Chem. Soc., Perkin Trans. 2*, 1986, 1623; (*c*) Y. Sakaino and R. Fujii, *J. Chem. Soc., Perkin Trans. 1*, 1990, 2852.

6 (*a*) T. H. Brehmer, P. P. Korkas and E. Weber, *Sensors and Actuators B*, 1997, **44**, 595; (*b*) Z. Fei, N. Kocher, C. J. Mohrschladt, H. Ihmels and D. Stalke, *Angew. Chem. Int. Ed.*, 2003, **42**, 783; (*c*) J. L. Scott, T. Yamada and K. Tanaka, *New J. Chem.*, 2004, **28**, 447.

7 (*a*) K. Yoshida, J. Yamasaki, Y. Tagashira and S. Watanabe, *Chem. Lett.*, 1996, 9; (*b*) K. Yoshida, T. Tachikawa, J. Yamasaki, S. Watanabe and S. Tokita, *Chem. Lett.*, 1996, 1027.

8 (*a*) K. Yoshida, H. Miyazaki, Y. Miura, Y. Ooyama and S. Watanabe, *Chem. Lett.*, 1999, 837; (*b*) K. Yoshida, Y. Ooyama, S. Tanikawa and S. Watanabe, *Chem. Lett.*, 2000, 714; (*c*) K. Yoshida, Y. Ooyama, H. Miyazaki and S. Watanabe, *J. Chem. Soc., Perkin Trans. 2*, 2002, 700–707; (*d*) K. Yoshida, Y. Ooyama, S. Tanikawa and S. Watanabe, *J. Chem. Soc., Perkin Trans. 2*, 2002, 708–714.

9 K. Yoshida, K. Uwada, H. Kumaoka, L. Bu and S. Watanabe, *Chem. Lett.*, 2001, 808.

10 (*a*) E. Weber and M. Czugler, in *Molecular and Molecular Recognition-Clathrates I and II*, ed. E. Weber, in *Top. Curr. Chem.*, Springer-Verlag, Berlin, 1988, vol. 149, p. 45; (*b*) E. Weber, in *Inclusion Phenomena and Molecular Recognition*, ed. J. L. Atwood, Plenum Press, New York, 1990, Vol. 4, p. 188.

11 F. Toda, *Acc. Chem. Res.*, 1995, **28**, 480.

12 K. Ochiai, Y. Mazaki, S.-I. Nishikiori, K. Kobayashi and S. Hayashi, *J. Chem. Soc., Perkin Trans. 2*, 1996, 1139.

13 (*a*) K. Hirano, S. Minakata and M. Komatsu, *Bull. Chem. Soc. Jpn.*, 2001, **74**, 1567; (*b*) K. Hirano, S. Minakata, M. Komatsu and J. Mizuguchi, *J. Phys. Chem. A*, 2002, **106**, 4868.

14 G. R. Desiraju, I. C. Paul and D. Y. Curtin, *J. Am. Chem. Soc.*, 1977, **99**, 1594.

15 M. Tanaka, H. Matsui, J. Mizuguchi, S. Kashino and K. Mogi, *Bull. Chem. Soc. Jpn.*, 1994, **67**, 1572.

16 (*a*) J. H. Kim, S. R. Shin, M. Matsuoka and K. Fukunishi, *Dye Pigm.*, 1999, **41**, 183; (*b*) K. Shirai, M. Matsuoka, S. Matsumoto and M. Shiro, *Dye Pigm.*, 2003, **56**, 83.

17 Y. Ooyama, T. Nakamura and K. Yoshida, *New J. Chem.*, 2005, **29**, 447–456.

18 teXsan: Crystal Structure Analysis Package, Molecular Structure Corporation, The Woodlands, TX, 1985 and 1992.

19 A. Altomare, M. C. Burla, M. Camalli, M. Cascarano, C. Giacovazzo, A. Guagliardi and G. Polidori, *J. Appl. Cryst.*, 1994, **27**, 435.

20 DIRDIF94. P. T. Beurskens, G. Admiraal, G. Beurskens, W. P. Bosman, R. de Gelder, R. Israel and J. M. M. Smits, *The DIRIF94 program system, Technical Report of the Crystallography Laboratory*, University of Nijmegen, The Netherlands, 1994.

21 M. C. Burla, M. Camalli, G. Cascaeano, C. Giacovazzo, G. Polidori, R. Spagna and D. Viterbo, *J. Appl. Crystallogr.*, 1989, **22**, 389.